A Difunctional Regeneration Scaffold for Knee Repair based on Aptamer-Directed Cell Recruitment

Xiaoxia Hu, Yulan Wang, Yaning Tan, Jie Wang, Haoyang Liu, Yingqian Wang, Shuang Yang, Miusi Shi, Shiyong Zhao, Yufeng Zhang, and Quan Yuan**

Articular cartilage is a translucent elastic connective tissue in the knee joint.[1] One end of the cartilage attaches to the subchondral bone and the other end faces the articular surface.[2] Unfortunately, damage to this tissue leads to knee joint dysfunction, resulting in significant pain and disability.[3] Since cartilage itself has no innate ability to mount a sufficient healing response, cartilage reconstruction remains a considerable challenge.[4] Recently, employing mesenchymal stem cell (MSC) transplants and then stimulating the directional differentiation into chondrocytes is becoming the method of choice for cartilage repair.[5,6] However, exogenous stem cell transplantation often causes problems in cartilage tissue engineering, such as lack of a targeted delivery system for MSCs, low survival rate of exogenous cells and the risk of exogenous infection due to the in vitro culture and proliferation of cells.[7–10] As a result, exogenous stem cell transplantation for cartilage repair has been significantly impeded. Simultaneously, clinical studies have shown that cartilage damage always extends deeply into the subchondral bone and thus causes osteochondral defects in the knee joint, which can alter the joint's biomechanical properties and influence the long-term performance of the cartilage tissue.[4] This fact indicates that the simultaneous repair of articular cartilage and the subchondral bone is important for successful knee repair. Since cartilage and subchondral bone have dissimilar tissue properties and regeneration abilities, repair of osteochondral defects is challenging.[11] Thus, there is a major need to develop a difunctional bilayer scaffold for recruitment of autologous MSCs and regeneration of osteochondral defects in the knee joint.

X. Hu, Y. Tan, J. Wang, H. Liu, Y. Wang, Prof. Q. Yuan
Key Laboratory of Analytical Chemistry for Biology and Medicine (Ministry of Education)
College of Chemistry and Molecular Sciences
Wuhan University
Wuhan 430072, China
E-mail: yuanquan@whu.edu.cn

Y. Wang, S. Yang, M. Shi, S. Zhao, Prof. Y. Zhang
State Key Laboratory Breeding Base of Basic Science of Stomatology (Hubei-MOST) and Key Laboratory of Oral Biomedicine
Ministry of Education
School and Hospital of Stomatology
Wuhan University
Wuhan 430079, China
E-mail: zyf@whu.edu.cn

Y. Wang, Prof. Y. Zhang
Medical Research Institute
School of Medicine
Wuhan University
Wuhan 430071, China

DOI: 10.1002/adma.201605235

Aptamers are short stretches of nucleotides or amino-acid residues, which can specifically recognize targets that vary from small molecules to cells.[12,13] The specificity and affinity of aptamers meet the requirements for detection, theranostics, and tissue engineering applications.[7,14,15] Recently, a DNA aptamer called Apt19S was developed to specifically recognize pluripotent stem cells.[16] However, research on the employment of the aptamer for recognition and further capture of MSCs for tissue engineering application has not been reported. An aptamer-directed repair system capable of selective recruitment of MSCs to the osteochondral defect site would open a new promising path for knee repair.

Due to the different requirements for cartilage and bone regeneration, it is a challenge to construct highly specialized scaffolds to mimic the structure of the osteochondral unit for supporting both cartilage and subchondral bone regeneration.[17–19] One means of meeting this challenge is via a bilayer scaffold composed of two different materials directed to the chondrogenic and osteogenic layers, respectively. Such a bilayer would improve regeneration of osteochondral defects in knee joints.[20,21] In this paper, we introduce an aptamer-functionalized bilayer scaffold (denoted as aptamer-bilayer scaffold) to achieve successful knee repair. As shown in **Scheme 1**, after designing the bilayer scaffold, aptamers specific to MSCs are immobilized on the scaffold to endow it with the capacity to capture MSCs. Then, the aptamer-bilayer scaffold is implanted into the osteochondral defect. The aptamer-functionalized gel layer (denoted as aptamer-gel) targets the cartilage defect for cartilage regeneration, while the aptamer-functionalized 3D graphene oxide (GO)-based biomineral framework (denoted as aptamer-GBF) layer is applied to the subchondral bone defect for bone regeneration. Because of the specific recognition and binding capability of the aptamer, this system can recruit endogenous MSCs from a marrow clot to the defect site. The stimulating factor kartogenin (KGN) in the aptamer-gel promotes chondrogenic differentiation of MSCs into chondrocytes, and the aptamer-GBF accelerates osteoblastic differentiation of MSCs into osteoblasts. Tests on rat knees showed that use of the aptamer-bilayer scaffold for osteochondral defect regeneration repaired the joints significantly. Considering the specific recognition of the aptamer for its target and the promising performance of the bilayer scaffold, our strategy paves the way to design new bioactive functional materials for tissue engineering and shows attractive prospects for targeted therapy.

Preparation of the aptamer-bilayer scaffold is shown in **Figure 1**a. GO as nanoscale filler is crosslinked into a sodium alginate (SA)-based network containing KGN to create a GO-SA gel for cartilage regeneration. Meanwhile, a 3D graphene

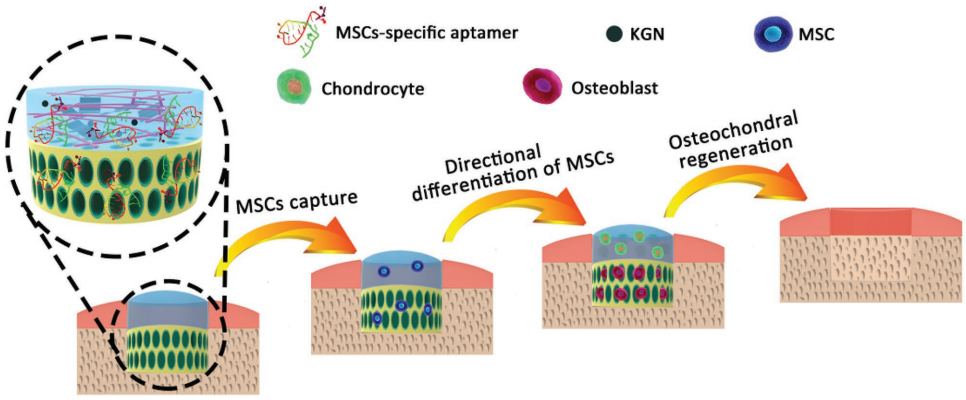

Scheme 1. Overview of aptamer-bilayer scaffold in osteochondral defect repair.

oxide-based biomineral framework (denoted as 3D-GBF) is designed for bone regeneration. The bilayer scaffold is then assembled from the GO-SA gel and 3D-GBF. Finally, MSC-specific aptamers are immobilized on the bilayer scaffold. The aptamer-gel has a well-defined and interconnected 3D porous network with pore diameters of hundreds of micrometers (Figure 1b), which is favorable for cell migration, cell proliferation, and ECM deposition.[5,22–24] No characteristic peak of GO at 10.6° was observed in the X-ray diffraction (XRD) pattern of the aptamer-gel (Figure S3, Supporting Information),

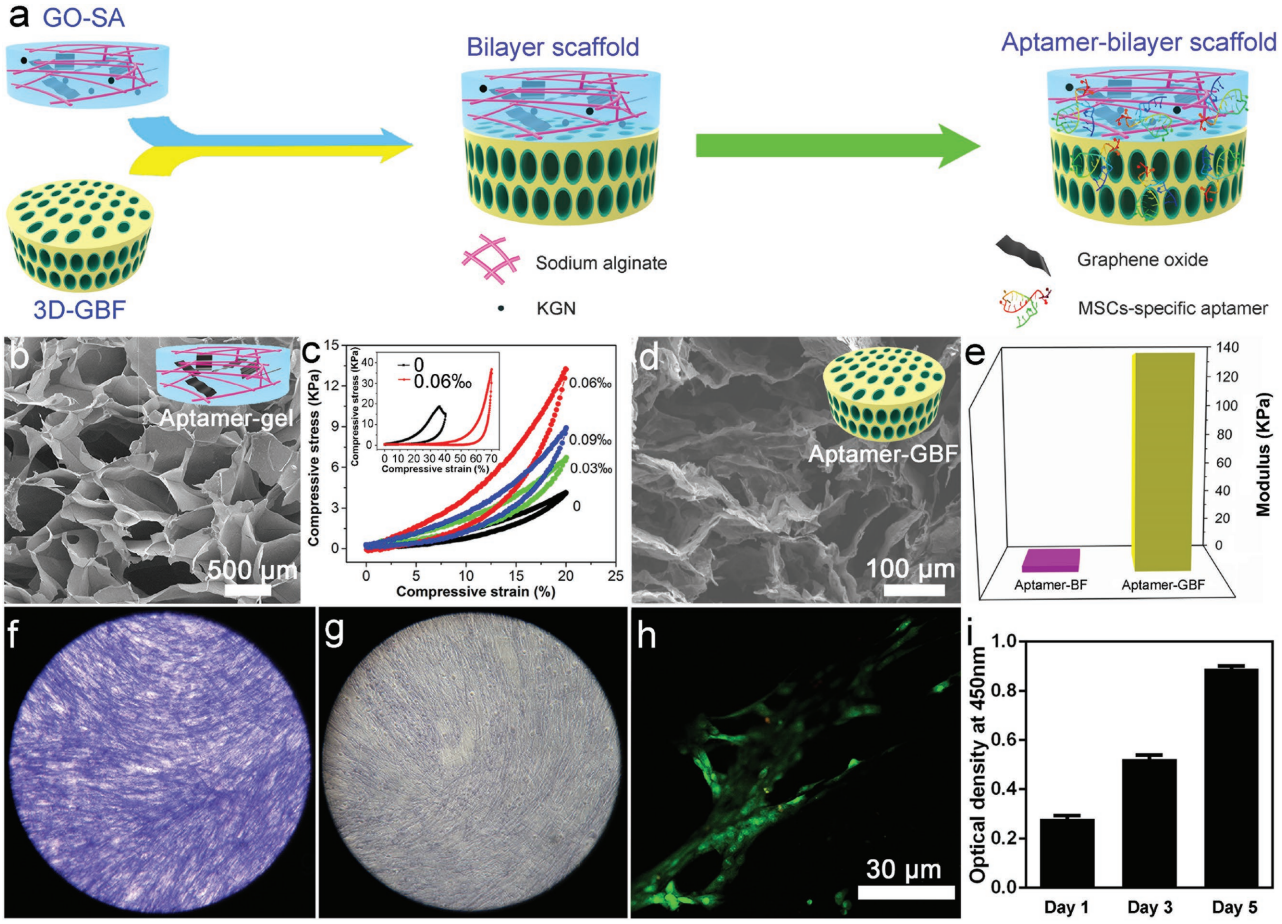

Figure 1. a) Preparation of the aptamer-bilayer scaffold. b) SEM image of the aptamer-gel. c) Compressive stress–strain curves of the aptamer-gels with different mass fractions of GO. Inset: compressive stress–strain curves of pure SA gels (black curve) and aptamer-gel containing 0.06% GO (red curve). d) SEM image of the aptamer-GBF. e) Young's modulus of the aptamer-BF and aptamer-GBF. ALP staining of MSCs cultured in the: f) aptamer-bilayer scaffold group and g) aptamer-gel group in normal induction media for two weeks. h) Confocal microscopy image of dead/live cell staining and i) the proliferation of MSCs in the aptamer-bilayer scaffold.

suggesting the absence of direct interaction or ordered stacking between GO sheets.[25] This result confirms that the GO sheets are well exfoliated and are homogeneously distributed in the gel matrix to enhance the mechanical properties of gel composites.[26] As shown in Figure 1c, compared to the gel without GO, the addition of 0.03% and 0.06% GO resulted in significant increases in compressive stress. However, the compressive stress of the aptamer-gel began to decrease when the amount of GO increased to 0.09%. These results indicate that a certain amount of GO can increase the compressive stress, whereas excess GO leads to reduced compressive stress. Additionally, the compressive strain of the aptamer-gel containing 0.06% GO reached 70% without collapse, while the SA gel readily broke at 40% compressive strain, indicating that the addition of GO dramatically improved the mechanical properties of the hydrogel. Likewise, the macrostructure and mechanical properties of the aptamer-GBF were investigated. The aptamer-GBF exhibited an interconnected macroporous network with a pore diameter of hundreds of micrometers (Figure 1d). The compressive Young's modulus of the aptamer-GBF was ≈135 kPa, while that of the aptamer-functionalized 3D biomineral framework (denoted as aptamer-BF) was ≈2 kPa (Figure 1e), demonstrating that graphene plays an important role in enhancing the mechanical properties of aptamer-GBF. The enhanced mechanical properties are promising for providing structural support to the newly formed bone tissue.

The sustained release of stimulating factor KGN can promote chondrogenic differentiation of stem cells.[27,28] The aptamer-gel demonstrated sustained-release behavior (Figure S6, Supporting Information), offering the possibility for controlled administration of KGN release in vivo, and thus accelerating chondrogenic differentiation of MSCs. In addition, the osteogenic potential of MSCs on aptamer-GBF was monitored. Compared with the aptamer-gel group, a higher level of alkaline phosphatase (ALP, the enzyme playing an essential role in bone mineralization) in the aptamer-bilayer scaffold group was observed (Figure 1fg). Also, ALP/total protein ratio was significantly upregulated in the aptamer-bilayer scaffold group compared with that in aptamer-gel group (Figure S7, Supporting Information). Furthermore, much more alizarin red-stained bone mineralized nodules were observed on the aptamer-bilayer scaffold compared to the aptamer-gel (Figure S8, Supporting Information). Therefore, it can be concluded that the aptamer-GBF part in the aptamer-bilayer scaffold plays an important role in accelerating the differentiation of MSCs toward the osteogenic lineage. The cell viability and morphology on the bilayer scaffold were analyzed to investigate its biocompatibility. As shown in Figure 1h, it is obvious that almost all cells were stained green and appeared to adhere well to the scaffold, indicating the high survival rate of MSCs on the scaffold. Additionally, MSCs maintained their spindle shape with good attachment to the scaffold surface (Figure S15, Supporting Information), verifying the excellent biocompatibility of this scaffold.[29] Furthermore, the number of MSCs in the aptamer-bilayer scaffold increased as time progressed (Figure 1i), demonstrating that the scaffold can promote the proliferation of cells. As a result, the aptamer-bilayer exhibits favorable properties for meeting the requirements of a knee repair scaffold, and exhibits high biocompatibility for cell survival as well as proliferation.

The aptamer-bilayer was able to recruit endogenous MSCs to the surface of the scaffold due to the recognition and binding ability of the MSC-specific aptamer Apt19S, as shown in **Figure 2**a. Fluorescence microscopy and flow cytometry were used to verify the specific binding of Apt19S with rat MSCs. As shown in Figure 2b, when FITC-labeled Apt19S was incubated with MSCs, strong green fluorescence was observed from the MSC surface. However, when incubated with rat osteoblasts, no fluorescence was observed, confirming the target role and high affinity of Apt19S. The targeting specificity of Apt19S toward MSCs was further confirmed by flow cytometry analysis (Figure 2c). When the FITC-labeled Apt19S was incubated with rat MSCs, strong fluorescence intensity was observed. In comparison, no fluorescence was observed after incubating the FITC-labeled Apt19S with fibroblasts. Thus, Apt19S exhibited much stronger binding affinity to rat MSCs compared to random cells. Furthermore, when the FITC-labeled Apt19S was incubated with whole bone marrow, a slight fluorescence enhancement was observed compared to the fibroblast group. This weak fluorescence intensity resulted from MSCs in the whole bone marrow. Therefore, a competitive recruitment of MSCs from the whole bone marrow was achieved. These results indicate that Apt19S possesses a strong binding affinity to rat MSCs, and it can specifically recognize and bind with MSCs in the whole bone marrow. It is widely accepted that recruitment of MSCs to the defect site is essential for knee repair, and the lack of MSC recruitment leads to poor healing.[30,31] In this case, the aptamer-bilayer scaffold was used for MSC capture and enrichment, and the in vitro binding of MSCs with this scaffold was examined. The number of cells which migrated to the aptamer-bilayer scaffold was much higher than the number in the bilayer scaffold without aptamer (Figure 2d,e). The statistical data showed that there were 122 ± 9 MSCs in the aptamer-bilayer scaffold, while only 61 ± 6 MSCs were in the bilayer scaffold without aptamer (Figure 2f). This transwell migration assay confirmed that the aptamer-bilayer scaffold showed better capability for MSC capture than the bilayer scaffold without aptamer. As a result, the immobilization of MSC-specific aptamer significantly improves MSC migration toward the scaffold, indicating that the aptamer provides a powerful tool for cell capture and enrichment.

Sprague Dawley rats were used as animal models to evaluate the knee repair capacity of the aptamer-bilayer scaffold. As shown in **Figure 3**a, a full-thickness rat osteochondral defect was first created in the knee joint. The scaffold was then implanted into the defect to test for improved tissue regeneration. After eight weeks healing, histomorphological analysis by safranin-O staining for glycosaminoglycans (GAG) and immunohistochemical staining for collagen type II were used to evaluate cartilage regeneration. Meanwhile, microcomputed tomography (μ-CT) reconstruction and hematoxylin and eosin (H&E) staining were performed on the articular joint samples to assess subchondral bone regeneration. As shown in Figure 3b, when the defect was treated with the aptamer-bilayer scaffold, fully hyaline-like cartilage was regenerated, as evidenced by strong safranin-O staining for GAG and immunohistochemical staining for collagen type II. The μ-CT reconstruction images showed that the subchondral bone defect was filled with newly regenerated bone tissue, and the new bone mainly regenerated

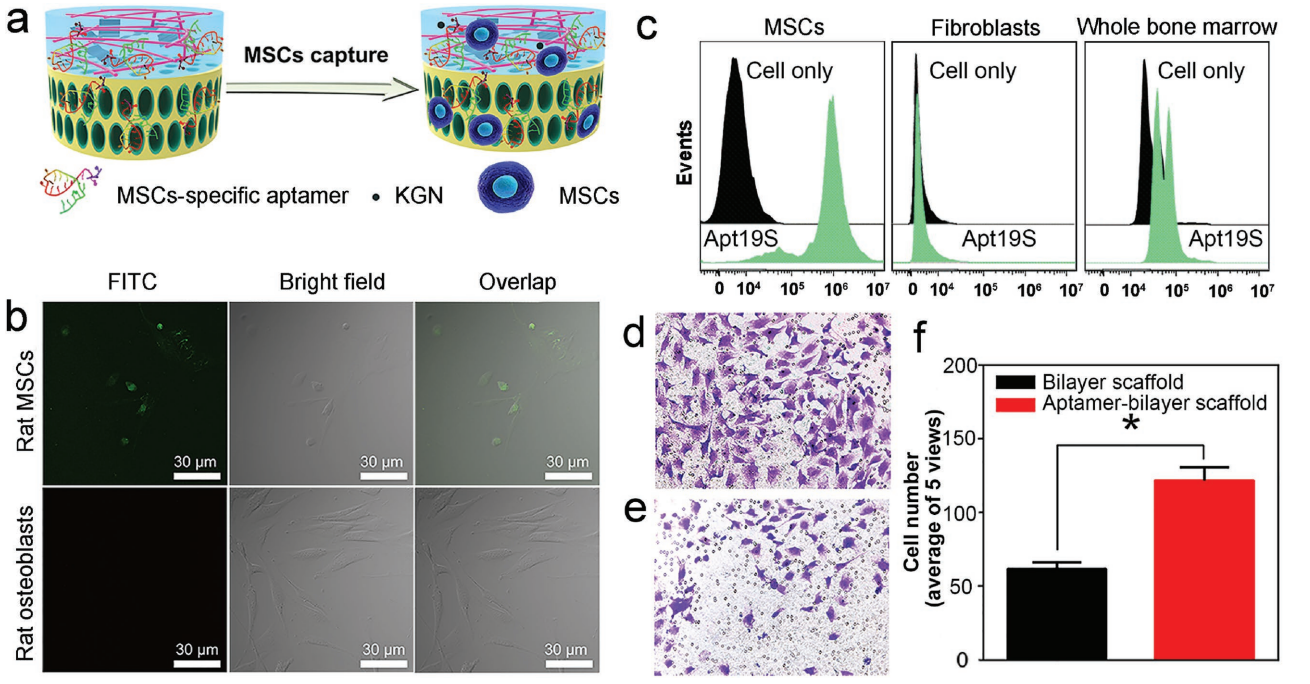

Figure 2. a) Schematic illustration of MSC recruitment based on the aptamer-bilayer scaffold. b) Confocal microscopy images of the binding of FITC-labeled Apt19S with rat MSCs and rat osteoblasts. c) Flow cytometry analysis of rat MSCs, fibroblasts, and whole bone marrow after incubation with FITC-labeled Apt19S. Light microscopy image of the transwell assay of MSCs toward the: d) aptamer-bilayer scaffold and e) bilayer scaffold. f) Statistical data of the transwell assay.

from the edge of defect toward the center (Figure 3c). Also, the H&E staining showed that a substantial amount of well-arranged new bone was formed (Figure 3d). In contrast, in the group treated with the bilayer scaffold, much weaker safranin-O staining and immunohistochemical staining were observed (Figure 3e). Additionally, there was less newly formed bone around the subchondral bone defect border, and the center of the defect remained empty (Figure 3f,g). Thus, the aptamer-bilayer scaffold demonstrated a superior capacity for osteochondral defect regeneration compared to the bilayer scaffold without aptamer, confirming that the MSC-specific aptamer with MSC recruitment ability exhibits outstanding performance for knee repair. When the defect was treated with the aptamer-gel, the regenerated tissue was stained positive with safranin-O, but was poorly stained with collagen type II antibody (Figure 3h). The cell density in the new tissue appeared lower compared to the aptamer-bilayer scaffold group (Figure S20, Supporting Information). For subchondral bone regeneration, there was minimal new bone formation around the defect border (Figure 3i,j). Therefore, the aptamer-bilayer scaffold showed better performance for osteochondral defect repair in comparison to the aptamer-gel. The results indicate that the bilayer scaffold aimed at both cartilage and the subchondral bone plays an important role in full knee repair. Neither the immunohistochemical staining nor the safranin-O staining was observed in the blank group without treatment (Figure 3k), and there was no obvious newly formed bone in the osteochondral defect (Figure 3l,m). Therefore, the osteochondral defect could not be repaired by self-healing. Furthermore, histological scoring evaluation was performed to evaluate the quality of the newly formed cartilage tissue after eight weeks healing. The aptamer-bilayer scaffold group had significantly higher score than the other groups for the predominantly hyaline-like cartilage (Figure 3n), verifying that the aptamer-bilayer scaffold has the best performance in neocartilage formation. The structural characteristics in Figure 3o showed that the neocartilage tissue in the aptamer-bilayer scaffold exhibited the best structural integrity among all the groups. Moreover, the regenerated cartilage was well bonded to the adjacent cartilage in the aptamer-bilayer scaffold group (Figure 3p). Furthermore, the highest bone formation percentage was observed in the aptamer-bilayer scaffold group, indicating that the amount of bone in this group was maximum (Figure 3q). The prospect of the aptamer-bilayer scaffold for knee repair was further evaluated after 12 weeks healing. The cartilage defect regeneration results at the 12th week were similar to those at the eighth week (Figures S22 and S23, Supporting Information). For the subchondral bone repair, the newly bone formation showed slight increase after 12 weeks treatment compared to that at eight weeks (Figures S24 and S25, Supporting Information). The results mentioned above demonstrate that the aptamer-bilayer scaffold exhibits best performance for osteochondral regeneration among all groups, confirming that the bilayer scaffold combined with the MSC-specific aptamer provides a powerful tool for successful osteochondral regeneration.

In this work, the MSC-specific aptamer integrated with the bilayer scaffold was successfully constructed for knee repair. The aptamer-bilayer scaffold not only specifically recognized and bound with MSCs, but also recruited MSCs to the bilayer scaffold, thus leading to enrichment of MSCs around the osteochondral defect. In addition, the bilayer scaffold exhibited advantages for osteochondral repair, such as the interconnected

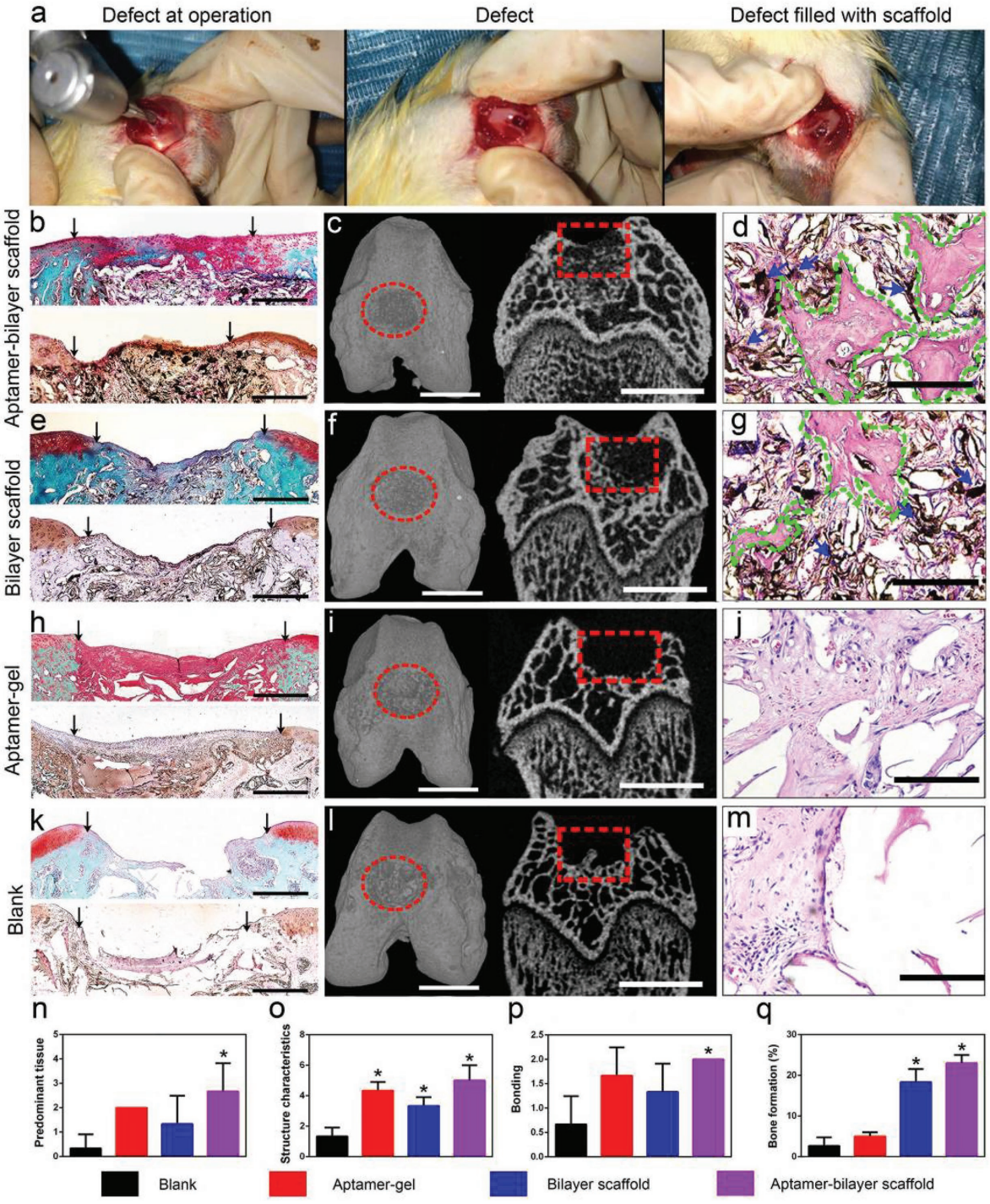

Figure 3. a) Scaffold implantation process. b) Histomorphological analysis of the neocartilage tissue. c) μ-CT reconstruction of the osteochondral defect and d) histomorphological analysis of the newly formed bone tissue after treatment with the aptamer-bilayer scaffold. e) Histomorphological analysis of the neocartilage tissue, f) μ-CT reconstruction of the osteochondral defect, and g) histomorphological analysis of the newly formed bone tissue after treatment with the bilayer scaffold. h) Histomorphological analysis of the neocartilage tissue, i) μ-CT reconstruction of the osteochondral defect, and j) histomorphological analysis of the newly formed bone tissue after treatment with the aptamer-gel. k) Histomorphological analysis of the neocartilage tissue, l) μ-CT reconstruction of the osteochondral defect, and m) histomorphological analysis of the newly formed bone tissue without treatment. n–p) Histological scoring evaluation of the neocartilage tissue. q) Percentage of bone formation. Scale bars represent 0.5 mm in (b), (e), (h), and (k); 2.0 mm in (c), (f), (i), and (l); and 100 μm in (d), (g), (j), and (m). The black arrows in (b), (e), (h), and (k) point to the interface areas between the repair tissues and the host cartilage. The red elliptical rings and red boxes in (c), (f), (i), and (l) represent the osteochondral defect. The blue arrows and green irregular shapes in (d), (g), (j), and (m) represent the scaffolds and newly formed bone tissues, respectively. All data represent the mean values ± standard deviation ($N = 3$, $^*p < 0.05$).

3D porous network for cell migration, excellent mechanical properties to support newly formed tissue, and the ability to stimulate the directional differentiation of MSCs. Therefore, this aptamer-bilayer scaffold showed excellent performance for osteochondral knee joint. Due to its recruitment of MSCs and its other outstanding properties, the bilayer design has been demonstrated to be a potential scaffold for knee repair and worthy of further investigation toward clinical application. This strategy can also serve as an effective approach for cell recruitment in targeted therapy and is anticipated to find broad application in regenerating new tissues and organs.

Supporting Information

Supporting Information is available from the Wiley Online Library or from the author.

Acknowledgements

X.H. and Yu.W. contributed equally to this work. This work was supported by the National Natural Science Foundation of China (51272186, 21422105, 81271108, and 81570954), A Foundation for the Author of National Excellent Doctoral Dissertation of P. R. China (201220), Ten Thousand Talents Program for Young Talents (to Quan Yuan), and the Fundamental Research Funds for the Central Universities (2015203020207, 410500041). Q.Y. thanks the large-scale instrument and equipment sharing foundation of Wuhan University. All surgical procedures used in these experiments were approved by the Ethics Committee for Animal Research, Wuhan University, China.

Received: September 28, 2016
Revised: November 25, 2016
Published online:

[1] A. J. S. Fox, A. Bedi, S. A. Rodeo, *Sports Health* **2009**, *1*, 461.
[2] V. C. Mow, A. Ratcliffe, A. R. Poole, *Biomaterials* **1992**, *13*, 67.
[3] A. Praemer, S. Furner, D. P. Rice, *Musculoskeletal Conditions in the United States*, American Academy of Orthopaedic Surgeons, Rosemont, IL, USA **1999**.
[4] S. Lopa, H. Madry, *Tissue Eng., Part A* **2014**, *20*, 2052.
[5] X. Liu, X. Jin, P. X. Ma, *Nat. Mater.* **2011**, *10*, 398.
[6] R. K. Das, V. Gocheva, R. Hammink, O. F. Zouani, A. E. Rowan, *Nat. Mater.* **2016**, *15*, 318.
[7] L. Chao, B. Guo, H. Wu, N. Shao, D. Li, J. Lin, L. Dang, C. Wang, L. Zhang, A. Lu, G. Zhang, *Nat. Med.* **2015**, *21*, 288.
[8] J. F. Liao, Y. Qu, B. Y. Chu, X. N. Zhang, Z. Y. Qian, *Sci. Rep.* **2014**, *5*, 09879.
[9] Y. Peck, P. F. He, G. S. V. N. Chilla, C. L. Poh, D. A. Wang, *Sci. Rep.* **2015**, *5*, 16225.
[10] D. J. Huey, J. C. Hu, K. A. Athanasiou, *Science* **2012**, *338*, 917.
[11] S. Vijayan, W. Bartlett, G. Bentley, R. W. J. Carrinner, R. C. Pollock, M. Alorjani, T. W. R. Briggs, *J. Bone Jt. Surg., Br. Vol.* **2012**, *94-B*, 488.
[12] X. Fang, W. Tan, *Acc. Chem. Res.* **2010**, *43*, 48.
[13] X. Xiong, H. Liu, Z. Zhao, M. B. Alman, D. Lopez-Colon, C. J. Yang, L. J. Chang, C. Liu, W. Tan, *Angew. Chem. Int. Ed.* **2013**, *52*, 1472.
[14] Q. Yuan, Y. Wu, J. Wang, D. Lu, Z. Zhao, T. Liu, X. Zhang, W. Tan, *Angew. Chem. Int. Ed.* **2013**, *52*, 13965.
[15] J. Wang, Y. Wei, X. Hu, Y. Fang, X. Li, J. Liu, S. Wang, Q. Yuan, *J. Am. Chem. Soc.* **2015**, *137*, 10576.
[16] Z. Hou, S. Meyer, N. E Propson, J. Nie, P. Jiang, R. Stewart, J. A Thomson, *Cell Res.* **2015**, *25*, 390.
[17] J. M. Oliveira, M. T. Rodrigues, S. S. Silva, p. b. Malafaya, M. E. Gomes, C. A. Viegas, I. R. Dias, J. T. Azevedo, J. F. Mano, R. L. Reis, *Biomaterials* **2006**, *27*, 6123.
[18] Y. Jiang, L. Chen, S. Chen, S. Zhang, T. Tong, W. Zhang, W. Liu, G. Xu, R. Tuan, B. C. Heng, R. Crawford, Y. Xiao, H. W. Ouyang, *Acta Biomater.* **2013**, *9*, 8089.
[19] J. P. Seo, T. Tanabe, N. Tsuzuki, S. Haneda, K. Yamada, H. Furuoka, Y. Tabata, N. Sasaki, *Sci. Vet. Sci.* **2013**, *95*, 1210.
[20] E. G. Lima, R. L. Mauck, S. H. Han, S. Park, K. W. Ng, G. A. Ateshian, C. T. Hung, *Biorheology* **2004**, *41*, 577.
[21] D. Schaefer, I. Martin, P. Shastri, R. F. Padera, R. Langer, L. E. Freed, G. Vunjak-Novakovic, *Biomaterials* **2000**, *21*, 2599.
[22] H. Bramfeld, G. Sabra, V. Centis, P. Vermette, *Curr. Med. Chem.* **2010**, *17*, 3944.
[23] N. Annabi, J. W. Nichol, X. Zhong, C. Ji, S. Koshy, A. Khademhosseini, F. Dehghani, *Tissue Eng., Part B* **2010**, *16*, 371.
[24] V. Karageorgiou, D. Kaplan, *Biomaterials* **2005**, *26*, 5474.
[25] Y. Xu, H. Bai, G. Lu, C. Li, G. Shi, *J. Am. Chem. Soc.* **2008**, *130*, 5856.
[26] L. Zhang, Z. Wang, C. Xu, Y. Li, J. Gao, W. Wang, Y. Liu, *J. Mater. Chem.* **2011**, *121*, 10399.
[27] K. Johnson, S. T. Zhu, M. S. Tremblay, J. N. Payette, J. N. Wang, L. C. Bouchez, S. Meeusen, A. Althage, C. Y. Cho, X. Wu, P. G. Schultz, *Science* **2012**, *336*, 717.
[28] J. Zhang, J. H.-C. Wang, *Bone Res.* **2014**, *2*, 14008.
[29] J. Lee, G. D. Lilly, R. C. Doty, P. Podsiadlo, N. A. Kotov, *Small* **2009**, *5*, 1213.
[30] Y. Wang, J. Zhu, H. F. DeLuca, *J. Bone Miner. Res.* **2014**, *29*, 685.
[31] D. Park, J. A. Spencer, B. I. Koh, T. Kobayashi, J. Fujisaki, T. L. Clemens, C. P. Lin, H. M. Kronenberg, D. T. Scadden, *Cell Stem Cell* **2012**, *10*, 259.